MILLIMETER GENERATION AND NONLINEAR PROPAGATION IN FERROMAGNETICS

Report Number 1

for

Contract DA 36-039 AMC-00041(E)

U. S. Army
Signal Research and Development Laboratory
Fort Monmouth, New Jersey

M. L. Report No. 1005

Prepared in accordance with
DA Project No. 3-99-21-001
Signal Corps Technical Requirements
No. SCL-5506B dated 8 December 1961

Approved by: H. J. Shaw

Microwave Laboratory
W. W. Hansen Laboratories of Physics
Stanford University
Stanford, California

ASTIA AVAILABILITY NOTICE

Qualified requestors may obtain copies of this report from ASTIA.

ASTIA release to OTS not authorized.

ARMED SERVICES TECHNICAL INFORMATION AGENCY
ARLINGTON HALL STATION
ARLINGTON 12, VIRGINIA

TABLE OF CONTENTS

ABSTRACT

1. The power output of the 50 Gc/s Type I generator has been increased to 10 milliwatts, and some progress has been made in measuring its output spectrum. A Type II generator has also been operated in the 50 Gc/s range.

2. On the theory of transient magnetization, an analytic formulation is given which is accurate for arbitrary pulsed field shape in the range of slow pulsed field rise.

3. Previous theoretical curves of harmonic spin wave suppression, showing discrimination between the spin wave and uniform precession modes, have been verified experimentally, through measurements of susceptibility curves, in the nonlinear range. An initial experimental investigation has been made of other means of spin wave suppression involving operation at frequencies slightly below the spin wave manifold.

4. Success has been achieved in the application of digital computer procedures to the problem of electromagnetic shock wave formation in ferrites. A numerical example of an application to pulse sharpening predicts very favorable results which may have important use in steepening of the initial rise of the dc field pulses for the Type II microwave generator. A final report on the formation and propagation of electromagnetic shock waves in ferrites is under preparation.

5. A new pulse-shaping procedure has given closer control of pulsed field shape, contributing to improvements in output power and spectrum of the Type I generator.

A procedure has been developed for determining the detailed shape of fast-rising pulsed fields which gives improved accuracy over previous methods when the pulsed field coil is very small.

6. Attempts at X-ray analysis of Zn_2Y disks at the Bragg angle have proved unsuccessful to date. Crystals grown by the Center for Materials Research have been verified to have Zn_2Y composition, and work is continuing toward the analysis and improvement of the quality of the crystals.

A. FACTUAL DATA

1. Pulsed Ferrite Millimeter Wave Generators

a. Type I Generator

During the past quarter special attention was given to the generator that yielded a 50 Gc/s signal with a 1 mwatt peak output power (Generator No. 6 of the Final Report under Contract DA 36(039) SC-85263). Special emphasis was placed on closer determination of the output frequency (it was known to be above the cutoff frequency of the RG99/U waveguide used in the setup described in Figs. 1.4 and 1.5 of that report) and on raising the output power.

One objective of the present work is to determine the output spectrum with reasonable accuracy, i.e., the distribution of output energy as a function of frequency. It appears that the most feasible approach to this problem at present is through tunable filter techniques. Scanning the spectrum with a suitable filter and properly reducing the data should produce the desired information.

One model of such a filter was built during the last quarter. It uses a rectangular waveguide having one of the side walls continuously variable, thus varying the cutoff frequency of the TE_{10} mode in the waveguide, such that $\lambda_c = 2a$, where a is the width of the rectangular waveguide and λ_c is the free space wavelength associated with the cutoff frequency.

The variable side wall is made up of a movable center piece which is connected to the fixed parts of this side wall by means of two transition pieces connected to the center length on one side and to the fixed parts on the other end. A micrometer screw drives the center length through an external notch, thus varying the width a of the waveguide at that position continuously and hence also the cutoff frequency. The dial setting of the micrometer screw may directly be calibrated in terms of frequency. This waveguide acts therefore as a high pass filter with continuously variable lower cutoff frequency. The entire waveguide is gold-plated before assembly, to insure good contacts between the movable and fixed parts and to minimize insertion loss.

An initial test of the operation of this device was performed, recording the output energy transmitted through the variable cutoff waveguide as a function of the dial setting. The energy was obtained by numerically integrating the observed output pulse as it was recorded on a photograph as, e.g., in Fig. 1.2b. The result of this integration, as a function of frequency, is plotted in Fig. 1.1.

The conclusion may be drawn that the frequency spectrum present in the output pulse is contained essentially between 50 and 56 Gc/sec. However, it is found that the shape of the output pulse changes somewhat with tuning of the filter. This indicates a back reaction of the filter on the ferrite. For an accurate analysis of the spectrum, this effect will need to be accounted for, which will be done by a combination of analysis and experimental refinement. Experimentally, the electrical length of the waveguide connecting the ferrite with the variable cutoff waveguide might be made sufficiently long so that the wave reflected from the filter will reach the ferrite only after all the energy has been delivered by the ferrite to the waveguide, i.e., the round trip time of the output pulse will be longer than the width of the pulse, which is approximately 20 nsec. This is not unfeasible, since the group velocity in the waveguide for the frequency range under consideration is less than about half of the velocity of light. Thus, the ferrite will see a matched load during its radiation time.

Secondly, attention was geared during the last quarter toward increasing the peak output power of this Type I generator in the 50 Gc/s range. Two means of establishing this were employed:

(1) The driving power was raised.

(2) The shape of the magnetic field pulse was optimized, thus decreasing the overall rise time of the pulse. This is described in more detail in Section 5 of this report.

One of the limitations of reaching a higher level of output power was stated in connection with column 10 of Table 1.I of the Final Report mentioned above: the "low frequency" driving magnetic field at the position of the ferrite sphere was very low, due to insertion loss in the S-band input circuitry, yielding a value of $\theta/\theta_{crit} \ll 1$. To overcome this drawback--at least partially--a high-power, CW, S-band source (4J64 magnetron) was used to drive the sample. The final setup used an incident driving power of 5 watts with a coupling match corresponding to a VSWR of 3.0.

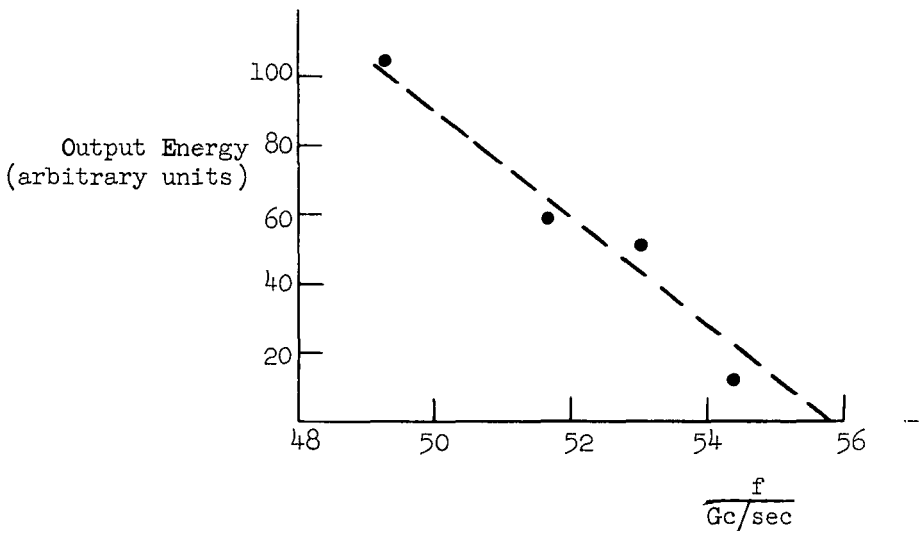
Output Energy
(arbitrary units)
100
80
60
40
20
48
50
52
54
56
f
Gc/sec

FIGURE 1.1

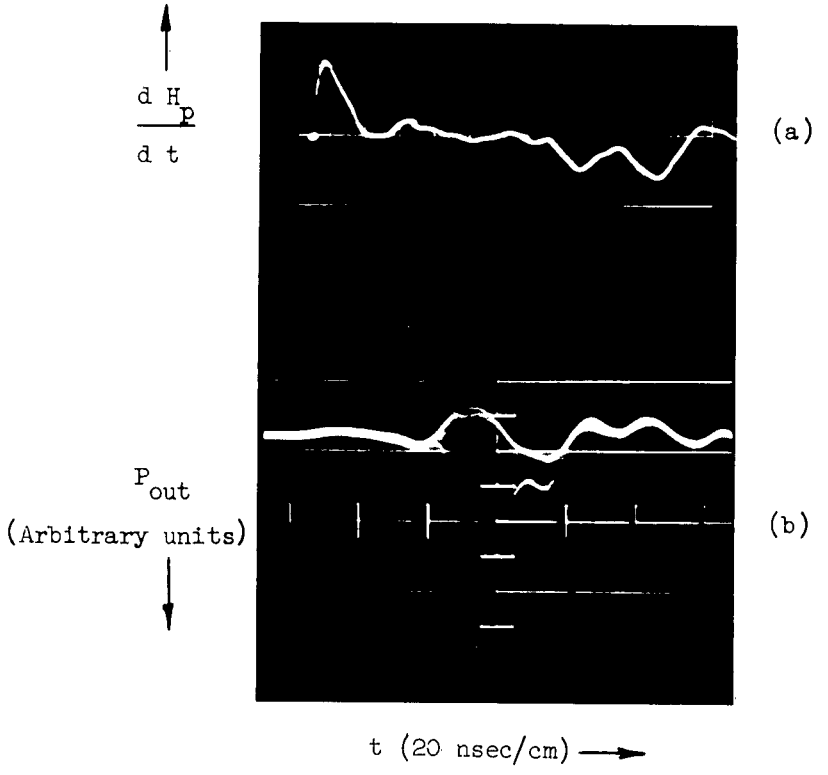

FIGURE 1.2

Using this higher power drive and the improved pulsed magnetic field, an output pulse with a peak power of about 10 mwatts was obtained. The differential of the applied pulsed magnetic field as it is displayed on the screen of the CRO is shown in Fig. 1.2a. This wave form was obtained using a pickup loop in the vicinity of the pulsing coil while the generator was operating. Figure 1.2b shows the observed output pulse which is detected through a crystal detector and fed to a CRO using a 30 db video amplifier. It will be noticed that the top trace of this picture is the reference line which is distorted due to stray pickup of the detection system. To obtain the actual output pulses, the difference has to be taken between the top trace and the pulse traces. Since the detector has a square-law characteristic in the operating range, the observed pulse shape is proportional to the square of the voltage seen by the detector and shows therefore directly the output power. The traces under the maximum pulse are obtained by sweeping the dc magnetic field through resonance at the driving frequency, the maximum pulse corresponding to resonant operation. For a fixed dc field, the output pulses show good stability.

b. Type II Generator

After the succesful operation of the Type I generator at frequencies in the 50 Gc/s range, the same output circuit as used above was tested in the Type II generator.

To achieve this, the same solenoid was used to generate the dc bias field in this case as was used in the Type I generator. The same output circuit configuration as before was employed, with the only difference being that it was immersed into the solenoid under an angle of about 15°. The bias field was adjusted to about 500 gauss and the pulsed field used in this setup was the same as shown in Fig. 1.2a.

This setup operated successfully, yielding a peak pulsed power output of about 1 mwatt with output pulse very similar in shape to the one shown in Fig. 1.2b, except for the lower amplitude. This constitutes the highest frequency obtained so far using a Type II setup and serves to show that generation of millimeter waves using this type of setup is feasible and should be investigated further.

2. Large Angle Theory of Transient Magnetization

Previously this study has been confined to the transient motion of the magnetization vector in isotropic spheres during the application of linear and piecewise-quadratic pulses of magnetic field. Our purpose here is to describe a generalization to general nonlinear pulse shapes. Referring to the fixed coordinate system (x'y'z') shown in Fig. 2.1, the sample is initially magnetized to saturation by a constant magnetic field with components

$$H_{x'} = H_0 \sin \psi_0 \tag{1}$$

$$H_{y'} = 0 \tag{2}$$

$$H_{z'} = H_0 \cos \psi_0 \quad . \tag{3}$$

A pulsed field, H_p , is then applied along the z' axis.

It is convenient to introduce the moving coordinate system (x, y, z) also shown in Fig. 2.1. The z-axis of this system is chosen to coincide with the total magnetic field, H , and the y-axis with the fixed system's y'-axis. The angle ψ is defined in the figure and ψ_0 is chosen to be the value of ψ at the initiation of the pulse.

The equations of motion in the moving coordinate system are given by

$$\frac{dM_x}{dt} = - \gamma M_y H - M_z \dot{\psi} \tag{4}$$

$$\frac{dM_y}{dt} = \gamma M_x H \tag{5}$$

$$\frac{dM_z}{dt} = M_x \dot{\psi} \quad , \tag{6}$$

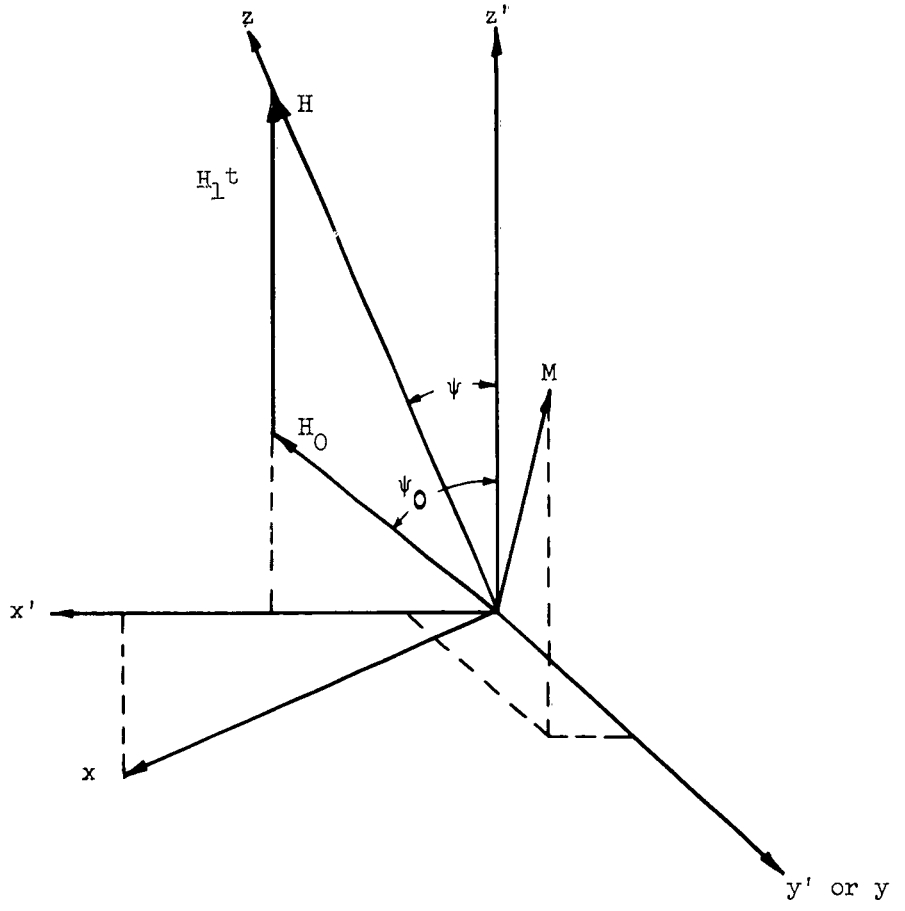

FIG. 2.1--Coordinate system.

where

$$H^2 = (H_0 \sin \psi_0)^2 + (H_0 \cos \psi_0 + H_p)^2 \tag{7}$$

$$\operatorname{ctn} \psi = \frac{H_0 \cos \psi_0 + H_p}{H_0 \sin \psi_0} \quad , \tag{8}$$

and

$$\dot{\psi} = - \frac{H_0 \sin \psi_0}{H^2} \frac{dH_p}{dt} \quad . \tag{9}$$

The initial conditions at $t = 0$ are:

$$M_x = M_y = 0 \tag{10}$$

$$M_z = 1 \quad . \tag{11}$$

If we assume that the pulse is rising slow enough to keep ϕ small, where ϕ is the precession angle, then M_z can be set to unity. If we introduce the new variable

$$m = M_x + iM_y \quad , \tag{12}$$

then the equations of motion reduce to

$$dm/dt = i \gamma H m + \frac{H_0 \sin \psi_0}{H^2} \frac{dH_p}{dt} \quad . \tag{13}$$

If we let

$$m = m_0 e^{i\lambda} \quad , \tag{14}$$

where

$$\lambda = \int_0^t \gamma H \, dt \quad , \tag{15}$$

then Eq. (13) reduces to

$$\frac{dm_0}{d\lambda} = \frac{H_0 \sin \psi_0}{\gamma H^3} \left(\frac{dH_p}{dt}\right) e^{-i\lambda} \quad . \tag{16}$$

By integrating, we obtain the solution

$$m_0 = \int_0^{\lambda} \frac{H_0 \sin \psi_0}{\gamma H^3} \frac{dH_p}{dt} e^{-i\lambda} \, d\lambda \quad . \tag{17}$$

Because the precession angle is small, it is given by

$$\phi = |m| = |m_0| \quad . \tag{18}$$

The final precession angle is given, therefore, by

$$\phi_\ell = \int_0^{\infty} \left| \frac{H_0 \sin \psi_0}{\gamma H^3} \frac{dH_p}{dt} e^{i\lambda} \, d\lambda \right| . \tag{19}$$

We now make an asymptotic expansion of Eq. (19) in inverse powers of H_0 by partial integration. The first integration by parts yields the relation

$$\phi_\ell = \left| \frac{\sin \psi_0}{\gamma H_0^2} \left(\frac{dH_p}{dt}\right)_{t=0} - \int_0^{\infty} \frac{d}{d\lambda} \left(\frac{H_0 \sin \psi_0}{\gamma H^3} \frac{dH_p}{dt}\right) e^{i\lambda} \, d\lambda \right| . \tag{20}$$

If the pulsing rate is slow, it seems plausible that the integral in this expression can be neglected. This premise is consistent with the results of a number of digital computer runs.

We obtain, therefore, as our final result, the expression

$$\phi_\ell = \left| \frac{\sin \psi_0}{\gamma H_0^2} \frac{dH_p}{dt} \right|_{t=0} \tag{21}$$

for the final precession angle. The expression holds for slowly-rising

nonlinear pulse shapes. In terms of computer studies mentioned in earlier reports, the condition of slow pulse-rise rate corresponds to the condition

$$\beta \gg 1 \quad , \tag{22}$$

where

$$\beta = \frac{\gamma H_0^2}{\left.\frac{dH_p}{dt}\right|_{t=0}} \quad .$$

For example, when β is 10, accuracies of the order of 1 - 2% are obtained in ϕ_ℓ .

3. Spin Wave Suppression

In the previous report[1] two schemes for spin wave suppression which are being investigated in this laboratory were summarized up to date. One scheme involves a process of parametric depumping of the spin waves. The other scheme involves operation of the uniform precession mode slightly below the bottom of the spin wave manifold. Work on both schemes has been continued during the past quarter, and the progress is described below.

On the first scheme, the previous report analyzed the effect of the pumping field, having twice the frequency of the uniform precession, on both the uniform precession and the spin wave mode, as a function of magnitude and phase of the parallel pumping field. The phase refers to the relative phase between the parallel pumping field and the perpendicular driving field, which is at a frequency equal to the uniform precession. The result of the analysis was plotted as in Fig. 3.2 of the previous report.[1] An important result from those curves is the fact that, under proper circumstances, it is seen possible to have a large depumping effect upon the spin wave concurrent with zero effect upon the uniform precession mode. This is a very favorable circumstance, as explained in the previous report.

Experiments have been performed during the past quarter to check quantitatively these theoretical curves. This involves determining experimentally $(\eta_0)_{eff}/\eta_0$ and $(\eta_k)_{eff}/\eta_k$ as a function of phase angle δ, for a fixed magnitude of parallel pumping field (h_2). Notations used here are the same as in the previous report. From these curves the increase in Θ_{crit} obtainable with this scheme of spin wave suppression is determined. The experimental setup has been described in the previous report. The process of determining $(\eta_0)_{eff}/\eta_0$ and $(\eta_k)_{eff}/\eta_k$ is to be described below.

The $(\eta_0)_{eff}/\eta_0$ is obtained from measurements of susceptibility at small signal levels (perpendicular driving field far below Suhl threshold); (η_0)eff and η_0 correspond respectively to measurements with and without

---

[1]Final Report under Contract DA 36(039) SC-85263, Microwave Laboratory Report No. 989, Stanford University (January 1963).

a parallel pumping field. The magnitude of the parallel pumping field used in the experiment is 7 oe.

The $(\eta_k)_{eff}/\eta_k$ is determined from the following relation:

$$\frac{(\eta_k)_{eff}}{\eta_k} = \frac{\left[\frac{(h_c)_{pump}}{(h_c)_{no\ pump}}\right]^2}{\left[\frac{(\eta_0)_{eff}}{\eta_0}\right]^2} \quad ,$$

where $(h_c)_{pump}$ and $(h_c)_{no\ pump}$ are the critical fields of the second order Suhl threshold, for cases with and without the presence of a parallel pumping field, respectively. This relation is derived from the well-known fact that the critical field is proportional to $\eta_0\sqrt{\eta_k}$. The critical fields for both the "pump" and "no pump" cases are determined experimentally from the decline of their susceptibility curves at high power levels. With these known values of $(h_c)_{pump}/(h_c)_{no\ pump}$, and $(\eta_0)_{eff}/\eta_0$, as determined previously, $(\eta_k)_{eff}/\eta_k$ is readily obtained from the above equation.

It should be noted that the above obtained values of $(\eta_0)_{eff}/\eta_0$ and $(\eta_k)_{eff}/\eta_k$ correspond to one certain value of δ , the phase angle between the parallel pumping and the perpendicular driving field. To obtain $(\eta_0)_{eff}/\eta_0$ and $(\eta_k)_{eff}/\eta_k$ as a function of δ , the above process is repeated for different values of δ . The work is obviously tedious, especially for the determination of $(\eta_k)_{eff}/\eta_k$. As a result, experiments were performed to obtain only enough points of $(\eta_k)_{eff}/\eta_k$ to show the main portion of the complete curve.

The results of the experiments are shown in Fig. 3.1. It shows good agreement with the curves predicted theoretically [(Fig. 3.2) of previous report]. The main interesting feature of the experimental curves is that they indeed prove that a certain phase angle δ , the parallel pumping field has a depumping effect upon the spin wave, while it has no effect on the uniform precession mode.

The maximum and minimum values of $(\eta_0)_{eff}/\eta_0$ and $(\eta_k)_{eff}/\eta_k$ are given respectively by $1 \pm \epsilon_0$ and $1 \pm \epsilon_k$ (previous report). The values of ϵ_0 and ϵ_k are thus derived from Fig. 3.1 to be approximately equal to 0.4 and 0.3, respectively. This means that, with the 7 oe pumping field

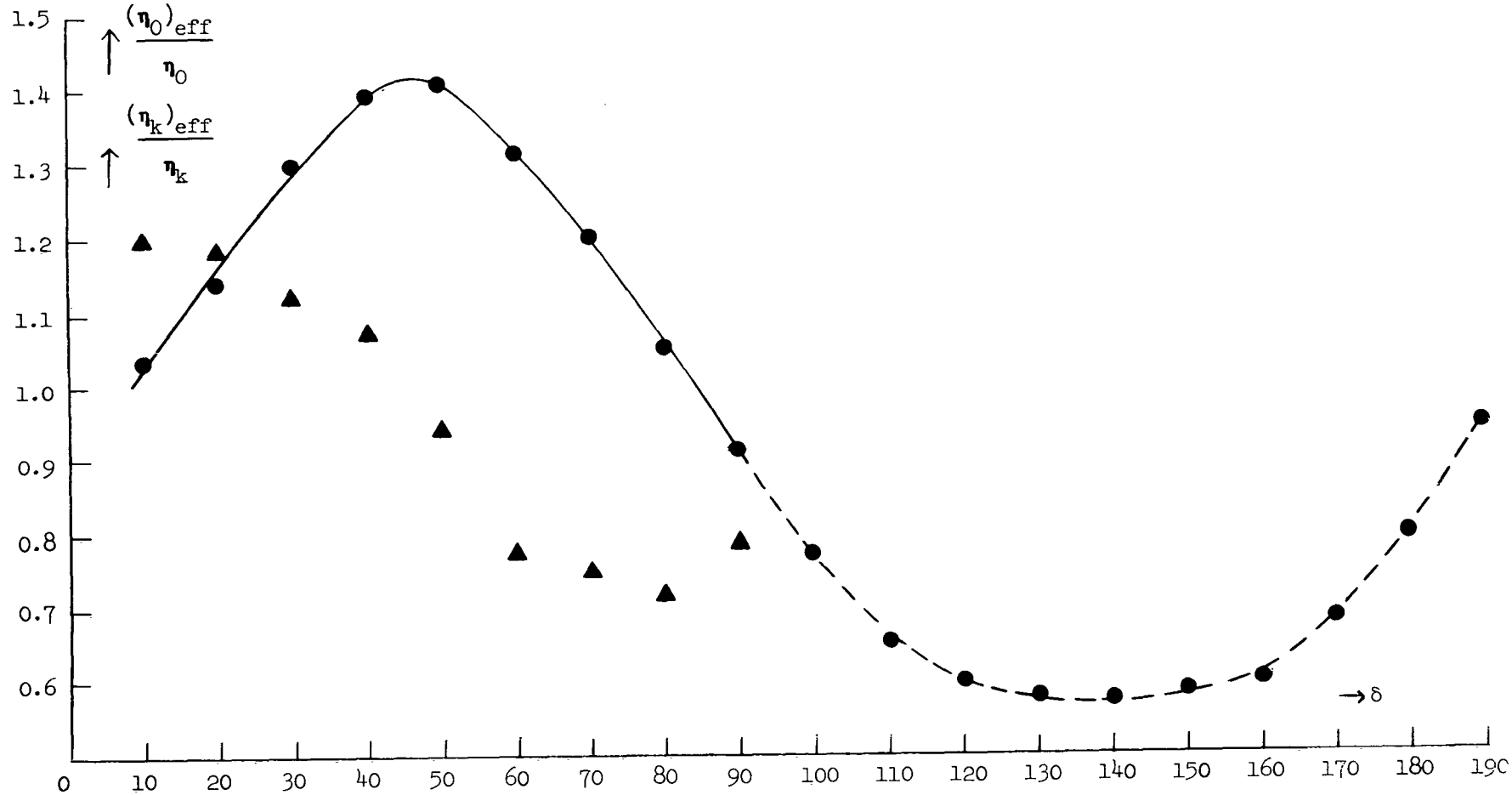
1.5
1.4
1.3
1.2
1.1
1.0
0.9
0.8
0.7
0.6
$\frac{(\eta_0)_{eff}}{\eta_0}$
$\frac{(\eta_k)_{eff}}{\eta_k}$
0
10
20
30
40
50
60
70
80
90
100
110
120
130
140
150
160
170
180
190
→δ

FIGURE 3.1

used in the present experiments, the effective spin wave linewidth has increased by approximately 30 per cent; the critical field, and hence also the critical angle, have increased by 17 per cent; and the energy stored in the uniform precession has increased by 30 per cent.

For other values of pumping field, these values would vary approximately proportionally to the pumping field amplitude.

As for the other scheme of spin wave suppression, namely, the one which involves operation of the uniform precession mode slightly below the bottom of the spin wave manifold, there are two possible types of operation as pointed out in the previous report. One type involves excitation of the uniform precession at a frequency somewhat below its resonant frequency. The second type involves a resonant type of operation obtained by splitting the uniform precession resonance into two normal modes by the use of a coupled cavity resonator.

Previous experiments[1,2] have indicated initial evidence on the first type of operation, namely, increased second harmonic output from a ferrite frequency doubler was observed, when the drive frequency lay slightly below the bottom of the spin wave manifold. This experiment was performed on a polycrystalline hexagonal ferrite disk with $\Delta H = 300$ oersted. Calculations show that the planar ferrite sample used in the experiment was biased such that the uniform precession was about 750 Mc, or 180 oe above the bottom of the spin wave manifold. The maximum second harmonic output observed experimentally occurred at a bias field for the uniform precession. This indicates that the assumption of operation below the bottom of the spin wave manifold is qualitatively acceptable.

In order to shed further light on this matter, it is instructive to study the susceptibility curve (vs applied dc field), because one would expect to observe a change in slope of the susceptibility curve when the drive frequency moves toward and lies slightly below the bottom of the spin wave manifold. In general, one would expect a steeper slope on the high field side of the curve than on the low field side. Experiments have been

---

[1]Report No. 8 for Contract DA 36(039) SC-85263, Microwave Laboratory Report No. 876, Stanford University (December 1961).

[2]Report No. 9 for Contract DA 36(039) SC-85263, Microwave Laboratory Report No. 904, Stanford University (March 1962).

performed with the same sample used previously. The driving rf field is sufficiently high to obtain well-detectable second harmonic output. The results are plotted in Fig. 3.2. The curves are in general agreement with what is expected. An attempt will be made to verify the mechanism by means of a quantitative theoretical interpretation.

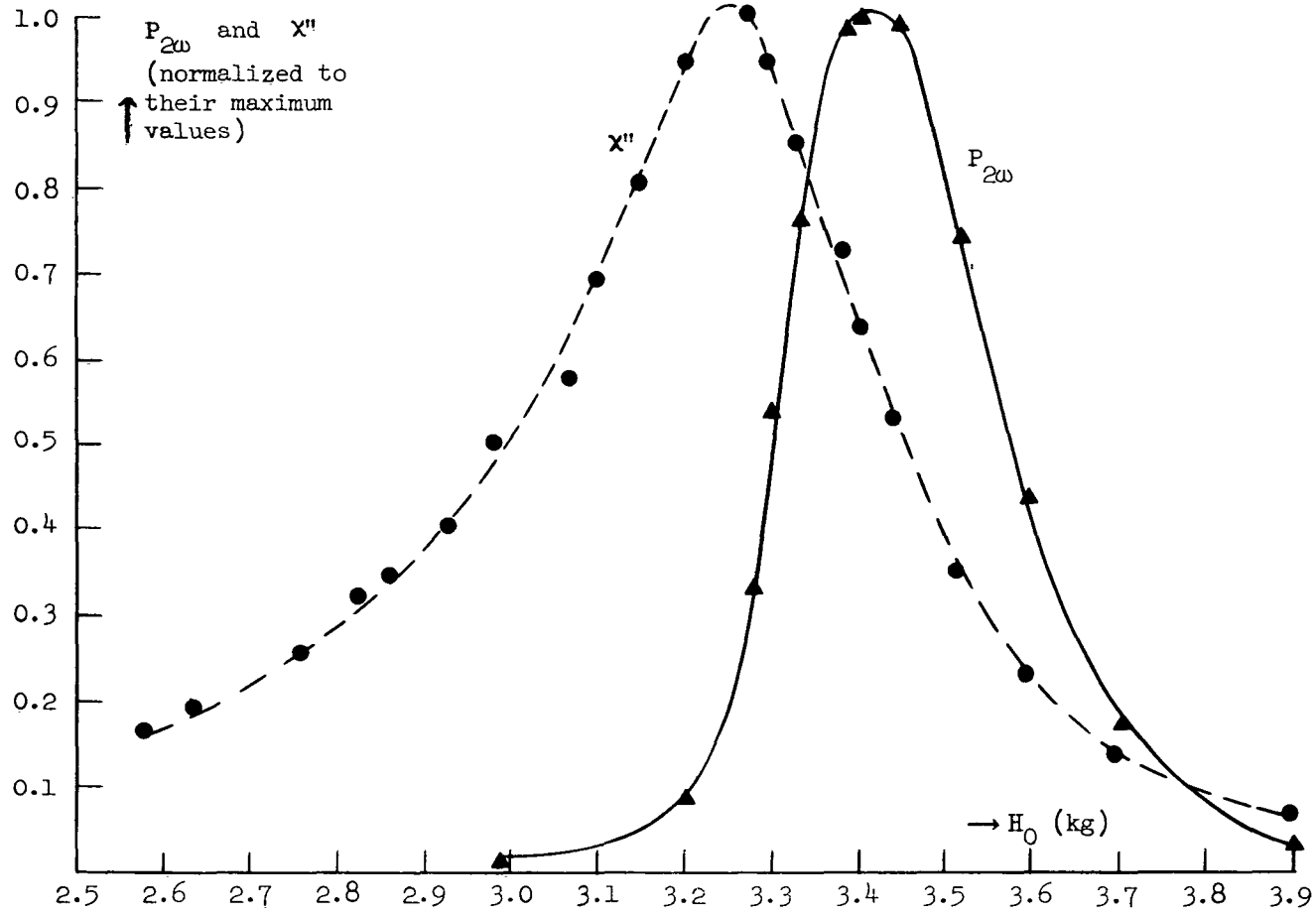
1.0
0.9
0.8
0.7
0.6
0.5
0.4
0.3
0.2
0.1
$P_{2\omega}$ and X"
(normalized to
their maximum
values)
X"
$P_{2\omega}$
H_0 (kg)
2.5
2.6
2.7
2.8
2.9
3.0
3.1
3.2
3.3
3.4
3.5
3.6
3.7
3.8
3.9

FIGURE 3.2

4. Shock Waves in Ferrites

During the past quarter work on this project has been concentrated on preparing a final report on the formation and propagation of electromagnetic shock waves in ferrites and upon obtaining numerical solutions to Maxwell's equations and the equation of motion for the magnetization. This latter work, which has been described in previous reports, has finally proved successful. The problem considered was that of a sloping-front step function composed of plane wave fronts propagating parallel to the external field in a semi-infinite, planar anisotropic ferrite. The y-z plane was taken as the easy plane. The result of a typical calculation is shown in Fig. 4.1, where the amplitude of the transverse field $h_t = (h_x^2 + h_y^2)^{1/2}$, normalized to the anisotropy field, H_a, is plotted against normalized time, $\gamma H_a t$, at a fixed point in space $(\gamma H_a \sqrt{\epsilon})/(c)\, z = 40$. The parameters chosen for the ferrite were $H_a = 10{,}000$ oe, $4\pi M = 3{,}000$ oe, α(loss parameter) $= 0.05$, $H_0 = 200$ oe. The wave form incident upon the ferrite medium at $z = 0$ was taken to be a pulse of the form

$$h_y(0,t) = \frac{h_0}{\tau_0} t \, , \quad h_x(0,t) = 0 \, ,$$

where $h_0 = 10{,}000$ oe, $\tau_0 = 1 \times 10^{-9}$ sec.

Also shown in Fig. 4.1 is the quasi-static approximation solution to the above problem (the quasi-static approximation is explained in detail in the Final Report of Contract DA 36(039) SC-85263), showing electromagnetic shock wave formation. Although time and memory limitations of the IBM 7090 computer made it unfeasible to carry the calculations any further than shown in Fig. 4.1, it is clear that the results of the exact solution are in good agreement with the quasi-static approximation and indicate that for the problem considered, a pulse with an initial rise time $\tau_0 = 10^{-9}$ sec will steepen until it becomes an electromagnetic shock wave with a shock front width of $\tau \approx 5 \times 10^{-11}$ sec.

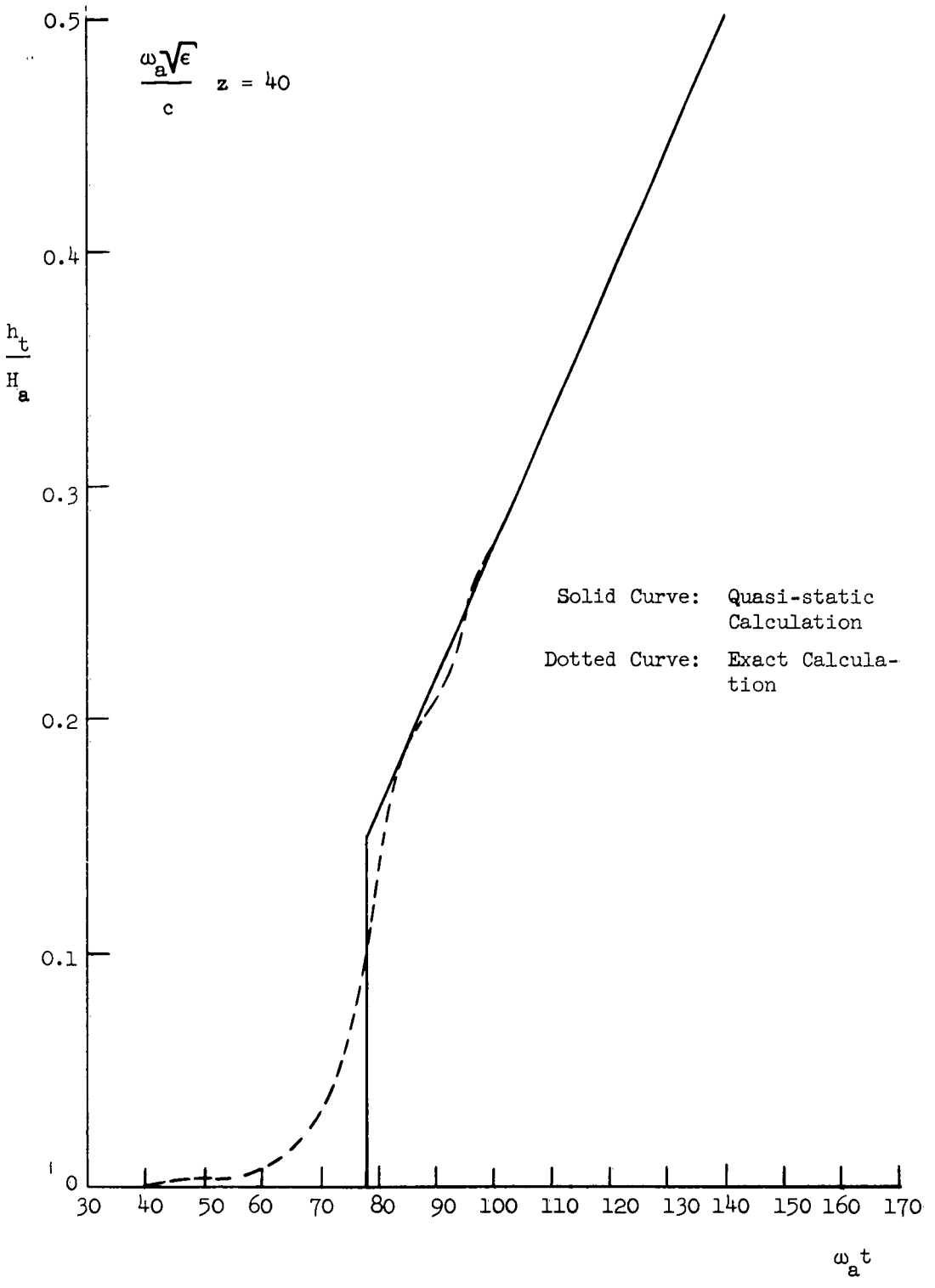
0.5
$\frac{\omega_a\sqrt{\epsilon}}{c}$ z = 40
0.4
$\frac{h_t}{H_a}$
0.3
0.2
0.1
0
30 40 50 60 70 80 90 100 110 120 130 140 150 160 170
$\omega_a t$
Solid Curve: Quasi-static Calculation
Dotted Curve: Exact Calculation

FIGURE 4.1

5. Pulsed Magnetic Fields

a. Control of Pulse Shape

During the past quarter some emphasis was put on further improvements on the rise time and flatness of the pulse shapes for pulsed field amplitudes in the order of 20 kgauss.

The basic setup used is the one described in connection with Generator No. 6 of the Final Report under Contract DA 36(039) SC-85263. Briefly, it consists of sets of 21 paralleled RG55/U coaxial cables that are charged to about 12 kv and discharged through a main gap and a sharpening gap into a three-turn copper strip pulsing coil. The shape of the magnetic pulse and its differential as it was used in the case of the No. 6 generator mentioned above is sketched in Fig. 5.1.

The object of the present adjustments was essentially to square up the upper edge a-b of the pulse as indicated by the dotted lines a-c-b , in order to improve the output spectrum and efficiency. This was achieved by inserting an additional set of coaxial lines on the output side of the sharpening gap. These lines were shorted on the free end and experimentally adjusted in length such as to cause reflections that would cancel out the portion d-e of the differentiated pulse, between about 20 and 60 nsec, in Fig. 5.1. This method was applied successfully and a pulse shape was obtained as shown in Fig. 5.2, whose differential is also shown in the photograph of Fig. 1.5a.

This method, even though it reduces the amplitude of the applied pulsed magnetic field since some of the energy stored in the charging section is lost to the 7 tuning lines, has proved to be valuable in controlling the pulse shape closely.

b. New Techniques for Determining the Detailed Shape of Fast Field Transients

As has been shown in previous reports, the detailed shape of the pulsed magnetic field $H_p(t)$ is important in the operation of the Type II microwave generator, particularly the shape during the initial portion of the pulse rise. It has also been shown that this field shape is difficult to measure for the case of the small pulsed field coils used with the higher frequency generators. In the procedure most often

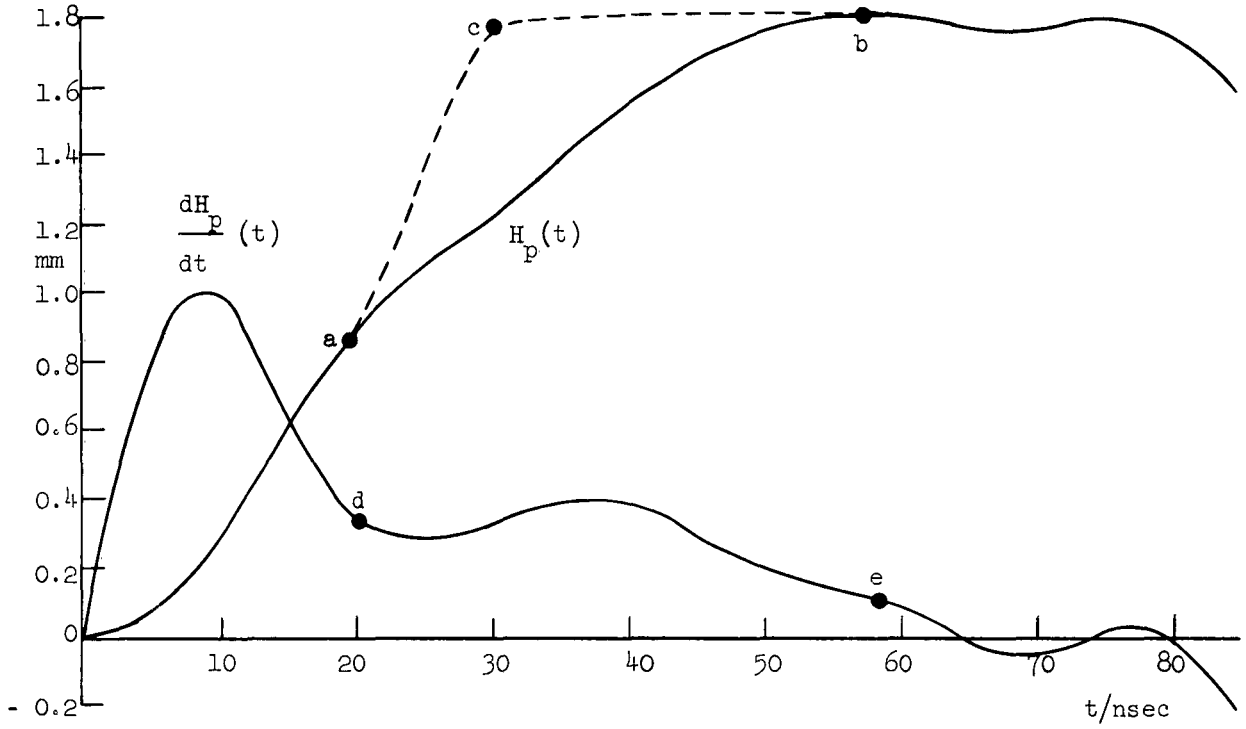

FIGURE 5.1

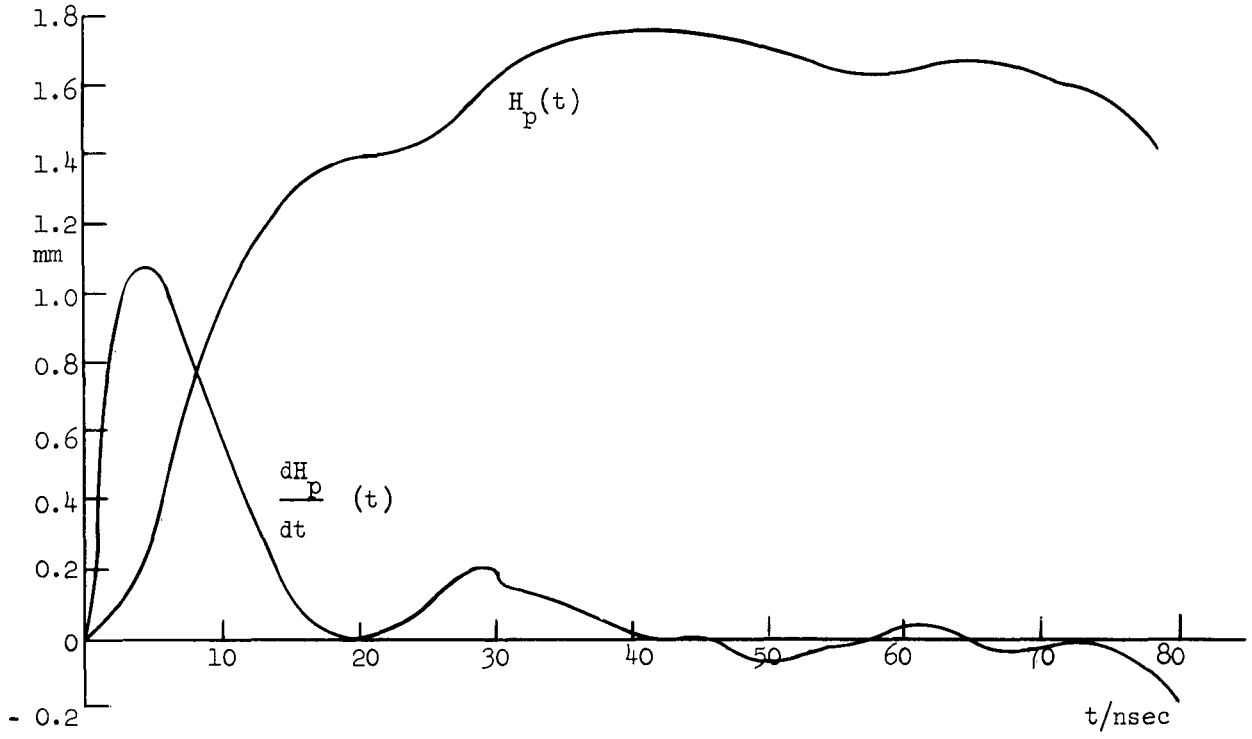

FIGURE 5.2

employed, a voltage $c(t)$, proportional to $dH_p(t)/dt$, is observed with the aid of a pick-up loop coupled to the pulsed field coil (which latter will be assumed to have inductance L) and a fast-response oscilloscope. After integration of $c(t)$, with corrections for the effect of the transient response of the oscilloscope, $H_p(t)$ becomes known.

Practical difficulties arise in applying this technique to the very small field-forming coils used in the high-frequency generators. Because of the low voltage sensitivity (9 volts/cm) of the fast oscilloscope used (Tektronix type 519, rise-time 0.28 nanoseconds), there is insufficient signal pick-up for adequate deflection.

By temporarily substituting a larger pulse-forming coil L_1 for the original coil L, this sensitivity problem can be overcome. It is then necessary, however, to have a new procedure for reducing the data and using it to infer the pulsed field characteristics associated with the coil L. For this purpose, the procedure described below has been developed.

It is necessary to determine firstly the equivalent, normalized, Thévenin voltage, $v(t)$, say, of the pulse-forming transmission line and gaps, then secondly, to find the coil current (and hence $H_p(t)$ which is directly proportional) for the case where original coil L is used. (This assumes that a section of isolating line separates the coil and the last spark gap.) The methods of carrying out these two operations will now be considered.

The Laplace-transformed Thévenin voltage $V(s)$ is the excitation function for the field-forming and observation system. The latter is characterized, in the s plane, by: (a) a zero at the origin to represent differentiation by the mutual coil coupling; (b) a pole at $-Z_0/L_1$ to represent the primary circuit transient response; and (c) a pole at $-2.2/t_r$ to represent the secondary circuit transient response, where t_r is the rise time of the oscilloscope and the time constant, L_2/R_2, of the secondary circuit is, by design, much faster than the primary time constant L_1/Z_0 and can, therefore, be neglected (L_2 is the

pick-up coil inductance, R_2 is the input resistance of the oscilloscope). Thus, the system function is

$$\frac{K_1 s}{(s + Z_0/L_1)(s + 2.2/t_r)} = \frac{K_1 s}{(s + a)(s + b)} , \qquad (1)$$

say, where K_1 is a constant of no immediate interest. In the s plane, the system output $C(s)$, which corresponds to our observed time function $c(t)$ is simply

$$C(s) = \frac{K_1 s V(s)}{(s + a)(s + b)} . \qquad (2)$$

Rearranging Eq. (2) in order to have the transformed unknown on the left gives

$$V(s) = \frac{(s + a)(s + b)}{K_1 s} C(s) = \left\{ \frac{(s + [a + b] + ab/s)}{k_1} \right\} C(s) . \qquad (3)$$

Now Eq. (3) may be solved for $V(s)$ and $v(t)$ found from $v(t) = \mathcal{L}^{(-1)}V(s)$ <u>only</u> if $c(t)$ is Laplace transformable. Pulse-forming apparatus that uses spark gap switching produces voltage transients with a single-valued waveform that are not accurately representable by the common time functions, such as the exponential build-up curve $(1 - e^{-t/T})$, ramp functions, parabolic buildup, etc. In order to evaluate Eq. (3), then, it is necessary to work in the time domain and employ convolution methods. Thus, inverse Laplace transforming (3) gives

$$v(t) = 1/K_1 \left\{ \delta'(t) + [a + b]\ \delta(t) + ab\ u(t) \right\} * c(t)$$

$$= 1/K_1 \left\{ (d/dt)\ c(t) + [a + b]\ c(t) + ab \int_0^t c(t)dt \right\} , \qquad (4)$$

where

$u(t)$ is the unit step function,

$\delta(t)$ is the unit delta function,

$\delta'(t)$ is the unit doublet function, and

$*$ represents convolution.

In this particular instance, direct use of the convolution integral is not required in the evaluation of $v(t)$. Instead, definite proportions of the observed quantity $c(t)$, its derivative and its integral are added, as prescribed by Eq. (4), to yield $v(t)$.

As an example, Fig. 5.3 shows $c(t)$ for a particular case,[1] as observed on the oscilloscope. Figure 5.4 shows $v(t)$ as derived from $c(t)$ as well as the simple integral of $c(t)$ for the sake of comparison.

The second part of the evaluation of $h_p(t)$ may now be carried out. A current $i(t)$ is produced by the Thévenin source $v(t)$, with source impedance Z_0 , in the coil L . But

$$i(t) = v(t) * \omega(t)$$

$$= \int_{-\infty}^{\infty} v(t - t')\, \omega(t')\, dt' \quad , \tag{5}$$

where $\omega(t)$ is the unit impulse (current) response of the coil circuit, i.e.,

$$\omega(t) = \mathcal{L}^{(-1)}\left[\frac{1}{sL + Z_0}\right] \quad , \tag{6}$$

or

$$\omega(t) = 1/L\, e^{-\frac{Z_0}{L} t} \quad . \tag{7}$$

Evaluation of the convolution integral, Eq. (5) is carried out by summing over small but finite time intervals $\Delta t'$ instead of integrating

[1] Final Report for Contract DA 36(039) SC-85263, Microwave Laboratory Report No. 989, Stanford University (January 1963), Generator No. 7, Table I.

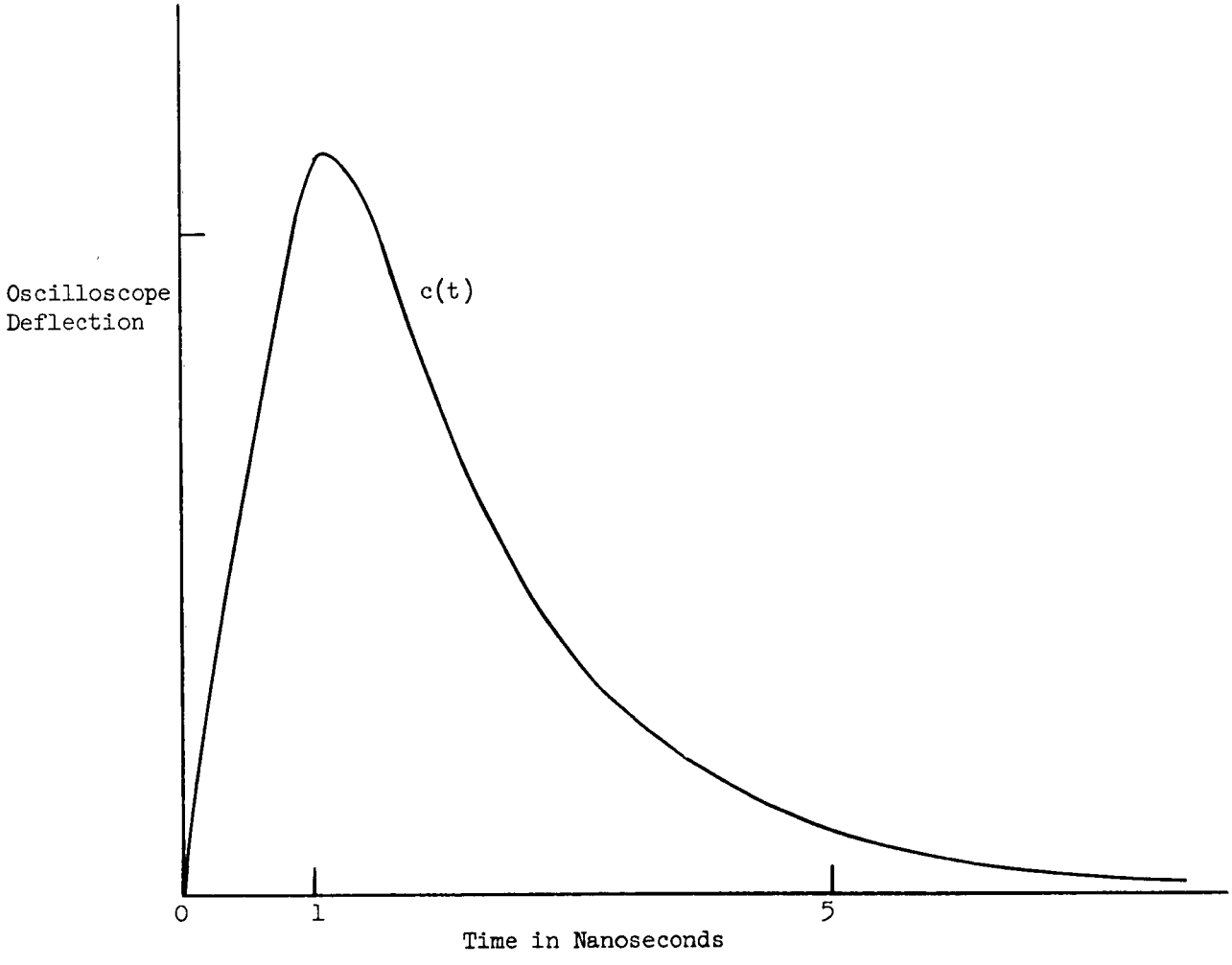

FIGURE 5.3

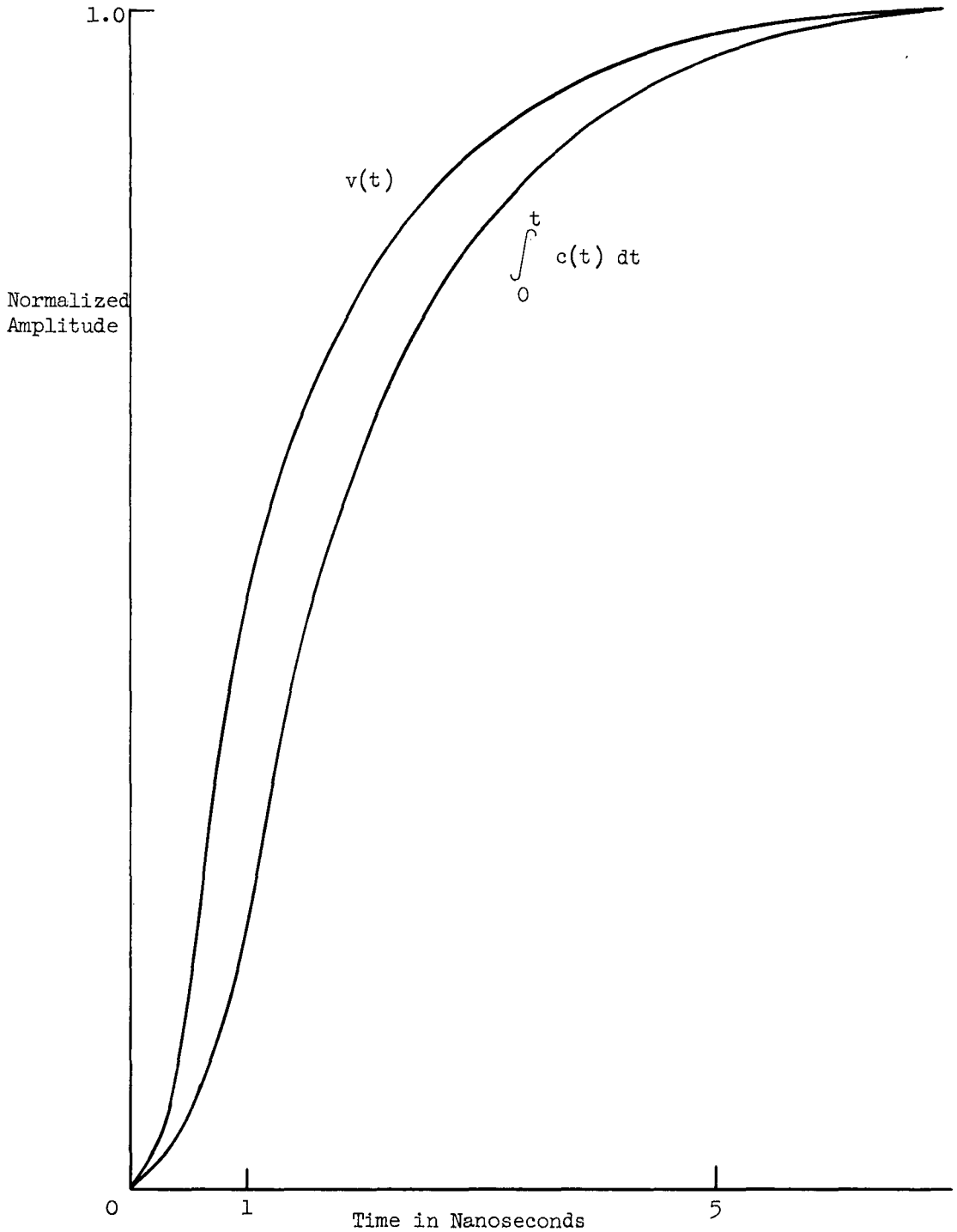
1.0
v(t)
$\int_0^t c(t)\,dt$
Normalized
Amplitude
0
1
5
Time in Nanoseconds

FIGURE 5.4

over infinitesimals dt' because $v(t)$ cannot be represented analytically. Accuracy is improved to the required degree by choosing sufficiently small $\Delta t'$. In the case in point the choice $\Delta t' = 0.05$ nanosec is adequate. The series-product method is used to evaluate the summation at several values of t which then gives points on the field waveform graph. Figure 5.5 shows the calculated initial part of the normalized field as used in the actual experiment.[1] For comparison, the faster-rising excitation voltage is also shown.

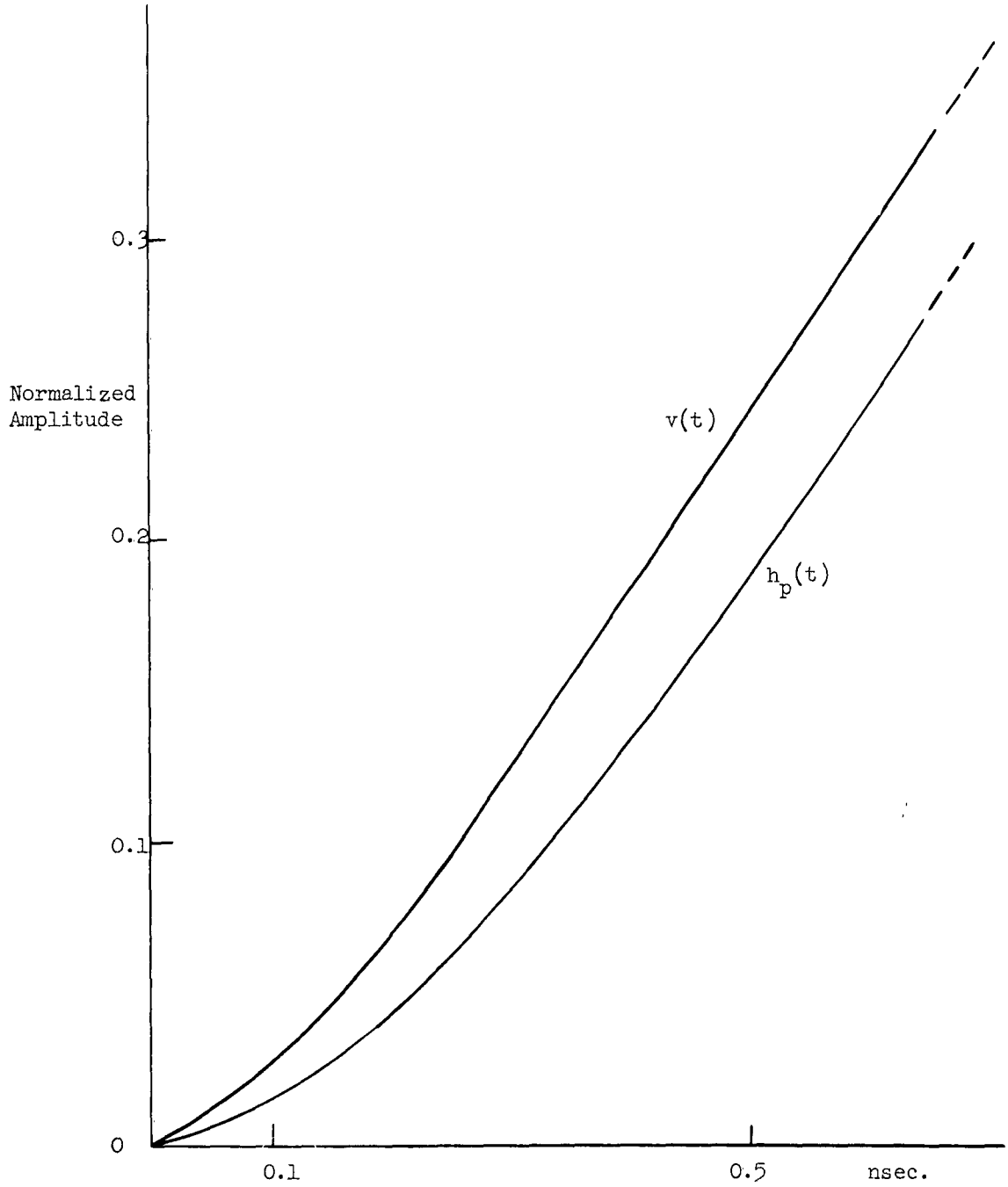

FIGURE 5.5

6. Sample Preparation

In the Final Report on Contract DA 36(039) SC-85263, mention was made of an x-ray technique for the detection of crystal defects, as described by Volkmar Gerold.[1] During this report period, several disks with suspected crystal defects were x-rayed in this manner, in an attempt to find the reason for the high linewidth.

First, the Bragg angle for Zn_2Y material was measured on an x-ray spectrometer. Subsequently, microradiographs were taken of suspected disks at the Bragg angle and the negatives were examined at 60 to 70 times magnification. Since the pictures showed no defects, the question was raised whether the tilting of the sample, when mounted in the goniometer, was accurate enough. Therefore, in a next attempt, a series of seven microradiographs was taken at angles of 0.3° increments above and below the Bragg angle in order to get an indication of the anomalous x-ray transmission which occurs at this angle. However, no anomalous transmission was found.

The most likely explanation for the apparent absence of the anomalous transmission is the high iron content of the ferrite which can lead to strong fluorescent radiation, excited by the incident x-ray beam, which in our case was predominantly 1.54 Angstrom (copper radiation, nickel filter). Further microradiographs will therefore be made using a wavelength that will not excite the iron in the ferrite, for instance, by using an iron anode x-ray tube.

The first batch of Zn_2Y crystals grown by the Center for Materials Research[2] were found, under electron microprobe analysis carried out by the Center, to have the correct composition. A second batch grown under slightly modified conditions was found to have ZnW composition. Modifications of the furnace are being made in preparation for further runs.

---

[1] Volkmar Gerold, Advances in X-Ray Analysis, Vol. 3, Plenum Press, 1960, p. 289.

[2] Under arrangements discussed in the Final Report for Contract DA 36(039 SC-85263.

B. CONCLUSIONS

1. Present indications are that reduction of input-circuit insertion loss in the Type I generator will result in further increase of power output. Present procedures for output spectrum analysis appear capable of refinements which will lead to better accuracy. No essential obstacles to extending the output frequencies of Type I and II generators beyond present values are foreseen at this time.

2. The theoretical study of the motion of magnetization in transient magnetic fields, in the absence of spin waves, has been completed. In previous reports, digital computer solutions have been given, over various normalized parameter ranges which cover all cases of practical interest. These are valid, for linear pulsed field rise, with arbitrary pulsing angle and arbitrary rise time. Complementing these are two asymptotic expressions, which complete the picture by giving good accuracy in two ranges where the numerical methods are least accurate, namely (1) the range of small pulsing angles, with arbitrary rise time, and (2) the range of slow pulse rise, for arbitrary pulsing angles, this latter case being the one covered in the present report. In this latter case, the pulsed field rise can be nonlinear. With these general approaches, then, all parameter ranges of interest are accurately covered, for cases where one works below the spin wave thresholds.

3. Harmonic spin wave suppression is capable of increasing the spin wave linewidth without affecting the uniform precession linewidth, in the predicted manner. Spin wave suppression by means of operation below the spin wave manifold shows promise of having the desired behavior.

4. The application of shock wave techniques to the sharpening of magnetic field pulses for the Type II microwave generator appears very promising at this time.

5. New attempts at more detailed control of pulsed-field shape appear to have been successful.

6. Chances for success in the Bragg angle x-ray analysis of Zn_2Y disks are not clear at this point.

C. PROGRAM FOR THE NEXT INTERVAL

1. Higher output frequency will be attempted with the Type I generator using output circuits suitable for the 75 Gc/s range. More precise determinations of output spectra will be undertaken. Attempts will be made at further increase of power output of the Type I and Type II generators in the 50 Gc/s range. In this connection an improved analysis of the input coupling problem for the Type I generator will be undertaken.

2. A technical report will be prepared on the completed first phase of the theoretical analysis of the transient motion of magnetization.

A second phase of the transient analysis will be undertaken, which will involve the inclusion of spin waves. The spin wave equations will be brought into the moving coordinate system, and methods of solving the resulting equations for the transient case will be studied.

3. Investigations will be continued on spin wave suppression by operation at frequencies below the spin wave manifold.

4. Work will continue on the final technical report on shock waves. Possible practical embodiments of a shock-wave type of pulsed-field steepener, for use with Type II microwave generators, will be studied.

5. It is not known at this time whether further pulsed-field work will be done during the coming quarter.

6. The study of Zn_2Y disks will continue during part of the coming quarter. Attempts will be made to pinpoint the source of linewidth anisotropy described earlier, by fabricating disks with minimum physical irregularities. Microwave analysis of new crystals produced by the Center for Materials Research will be undertaken.

KEY TECHNICAL PERSONNEL

(1 October 1962 to 31 December 1962)

H. J. Shaw	Responsible Investigator
B. A. Auld	Research Physicist
K. J. Harker	Research Physicist
M. S. Sparks	Assistant Professor
H. J. Landsbergen	Project Engineer
B. J. Elliott	Research Assistant
W. B. Hatfield	Research Assistant
G. L. Heiter	Research Assistant
S. G. Liu	Research Assistant
P. L. Young	Research Assistant

DISTRIBUTION LIST

Contract DA 36-039 AMC-00041(E)

OASD (R&E) 1
Attn: Technical Library
Rm. 3E1065, The Pentagon
Washington 25, D. C.

Advisory Group on Electron Devices 2
346 Broadway
New York 13, New York

Commanding Officer & Director 1
U. S. Navy Electronics Lab.
San Diego 52, California

Commander 1
Aeronautical Systems Division
Attn: ASAPRL
Wright-Patterson AFB, Ohio

Commander 1
Air Force Cambridge Research Laboratory
Attn: CRXL-R, Research Library
L. G. Hanscom Field
Bedford, Massachusetts

AFSC Scientific/Technical Liaison Office 1
U. S. Naval Air Development Center
Johnsville, Pennsylvania

Chief, U. S. Army Security Agency 2
Arlington Hall Station
Arlington 12, Virginia

Commanding Officer 1
U. S. Army Electronics Research Unit
P. O. Box 205
Mountain View, California

Commander 1
U. S. Army Missile Command
Attn: Technical Library
Redstone Arsenal, Alabama

Commander 20
Armed Services Technical Information Agnecy
Arlington Hall Station
Arlington 12, Virginia
Attn: TISIA

Director 1
U. S. Naval Research Lab.
Attn: Code 2027

Chief, Bureau of Ships 1
Department of the Navy
Attn: 681A-1
Washington 25, D. C.

Commander, AF Cambridge Research Laboratories 3
Attn: CCRR (1 cy)
CCSD (1 cy)
CRZC (1 cy)
L. G. Hanscom Field
Bedford, Massachusetts

Commander 1
Rome Air Development Center
Attn: RAALD
Griffiss Air Force Base,
New York

Chief of Research and Development 1
Department of the Army
Washington 25, D. C.

Deputy President 1
U. S. Army Security Agency Board
Arlington Hall Station
Arlington 12, Virginia

Commanding Officer 1
Harry Diamond Laboratories
Connecticut Ave. & Van Ness St. N.W.
Attn: Library, Rm. 211, Bldg. 92
Washington 25, D. C.

Commanding Officer 3
U. S. Army Electronics Command
Attn: AMSEL-AD
Fort Monmouth, New Jersey

Corps of Engineers Liaison Office 1
U. S. Army Electronics R & D Laboratory
Fort Monmouth, New Jersey

Commanding Officer 1
U. S. Army Electronics R & D Laboratory
Attn: Director of Research
Fort Monmouth, New Jersey

Commanding Officer 3
U. S. Army Electronics R & D Laboratory
Attn: Technical Information Division (FOR RETRANSMITTAL TO ACCREDITED BRITISH AND CANADIAN GOVERNMENT REPRESENTATIVES)
Fort Monmouth, New Jersey

Commanding Officer 1
U. S. Army Electronics R & D Laboratory
Attn: Logistics Division (For: SELRA/PRM, Project Engineer)
Fort Monmouth, New Jersey

Commanding General 1
U. S. Army Material Command
Attn: R & D Directorate
Washington 25, D. C.

Commanding Officer 1
U. S. Army Communication & Electronics Combat Development Agency
Fort Huachuca, Arizona

Director, Fort Monmouth Office 1
U. S. Army Communication & Electronics Combat Development Agency
Fort Monmouth, New Jersey

Commanding Officer 1
U. S. Army Electronics Material Support Agency
Attn: SELMS-ADJ
Fort Monmouth, New Jersey

Marine Corps Liaison Office 1
U. S. Army Electronics R & D Laboratory
Attn: SELRA/LNR
Fort Monmouth, New Jersey

Commanding Officer 1
U. S. Army Electronics R & D Laboratory
Attn: Technical Documents Center
Fort Monmouth, New Jersey

Commanding Officer 4
U. S. Army Electronics R & D Laboratory
Attn: SELRA/PR (Mr. Garoff)(1cy)
SELRA/PR (Mr. Hanley)(1cy)
SELRA/PRG (Mr. Zinn) (1cy)
SELRA/PRT (Mr. Kaplan)(1 cy)
Fort Monmouth, New Jersey

Commanding Officer 1
U. S. Army Electronics R & D
Attn: SELRA/PRM, Record File Copy
Fort Monmouth, New Jersey

Commanding General 1
U. S. Army Combat Developments Command
Attn: CDCMR-E
Fort Belvoir, Virginia

Hq. Electronic Systems Division 1
Attn: ESAT
L. G. Hanscom Field
Bedford, Massachusetts

AFSC Scientific/Technical Liaison Office 1
U. S. Army Electronics R & D Laboratory
Fort Monmouth, New Jersey

C. W. Barnes, Senior Research Engineer
Electron Devices Laboratory
Stanford Research Institute
Menlo Park, California — 1

Professor Donald C. Stinson
Electrical Engineering Department
University of Arizona
Tucson 25, Arizona — 1

Commanding Officer
Office of Naval Research, New York
Attn: A 10-2/IR:rf, Ser 5243
346 Broadway
New York 13, New York — 1

Micromega Corporation
4134 Del Rey Avenue
Venico, California
Attn: Dr. A. D. Berk — 1

Dr. T. Rossing
St. Olaf College
Northfield, Minnesota — 1

Dr. C. H. Holmes
Department of Electrical Eng.
Auburn University
Auburn, Alabama — 1

Mrs. Eunice P. Hazelton, Librarian
Sylvania Electronic Systems
Buffalo Operations
1100 Wehrle Drive
Buffalo 21, New York — 1

Stanford Research Institute
Menlo Park, California
Attn: Document Center — 1

Melabs, Inc.
3300 Hillview Avenue
Palo Alto, California
Attn: Dr. Vartanian — 1

Philips Laboratories
Irvington on Hudson
New York — 1

Commanding Officer
U. S. Army Electronics R & D Laboratory
Attn: SELRA/PEM (Isador Bady)
Fort Monmouth, New Jersey — 1

Research Division Library
Raytheon Company
28 Seyon Street
Waltham 54, Massachusetts — 1

Mauro DiDomenico, Jr.
Bell Telephone Laboratories
Murray Hill, New Jersey — 1

Prof. Arwin A. Dougal
Department of Electrical Eng.
University of Texas
Austin 12, Texas — 1

Air Force Cambridge Research Laboratories
L. G. Hanscom Field
Bedford, Massachusetts
Attn: F. A. Olson, CRRDA — 1